Ultrasensitive photodetectors based on monolayer MoS₂

Oriol Lopez-Sanchez¹, Dominik Lembke¹, Metin Kayci², Aleksandra Radenovic²* and Andras Kis¹*

Two-dimensional materials are an emerging class of new materials with a wide range of electrical properties and potential practical applications. Although graphene¹ is the most wellstudied two-dimensional material, single layers of other materials, such as insulating BN (ref. 2) and semiconducting MoS₂ (refs 3,4) or WSe₂ (refs 5,6), are gaining increasing attention as promising gate insulators and channel materials for fieldeffect transistors. Because monolayer MoS2 is a direct-bandgap semiconductor^{7,8} due to quantum-mechanical confinement^{7,9,10}, it could be suitable for applications in optoelectronic devices where the direct bandgap would allow a high absorption coefficient and efficient electron-hole pair generation under photoexcitation. Here, we demonstrate ultrasensitive monolayer MoS₂ phototransistors with improved device mobility and ON current. Our devices show a maximum external photoresponsivity of 880 A W⁻¹ at a wavelength of 561 nm and a photoresponse in the 400-680 nm range. With recent developments in largescale production techniques such as liquid-scale exfoliation¹¹⁻¹³ and chemical vapour deposition-like growth^{14,15}, MoS₂ shows important potential for applications in MoS2-based integrated optoelectronic circuits, light sensing, biomedical imaging, video recording and spectroscopy.

Molybdenum disulphide (MoS₂) is a typical semiconductor from the family of transition-metal dichalcogenide (TMD) materials with the common formula MX2, where M indicates a transition metal (M = Mo, W, Nb, Ta, Ti, Re) and X represents Se, S or Te. Bulk crystals of TMD materials are formed by vertically stacking two-dimensional layers with thicknesses of \sim 6.5 Å. Neighbouring layers are weakly bound by van der Waals interactions, facilitating cleavage of bulk crystals either using the micromechanical cleavage technique^{1,3} commonly used for the production of graphene, or liquid-phase exfoliation^{11–13}. Large-area MoS₂ can also be grown using chemical vapour deposition (CVD)-like growth techniques^{14,15}. Within the layers, chalcogenide and metal atoms are strongly bound via covalent bonds, resulting in MoS₂ membranes¹⁶ with mechanical strengths 30 times higher than that of steel¹⁷ and stability up to 1,100 °C in an inert atmosphere. The bandgap of MoS₂ can be tuned by varying the number of layers in the crystal. Bulk MoS₂ is an indirect-gap semiconductor with a bandgap of 1.2 eV (ref. 18), whereas single-layer MoS₂ is a direct-gap semiconductor⁷⁻¹⁰ with a bandgap of 1.8 eV (ref. 8), as a result of quantum confinement¹⁰. Because monolayer MoS₂ has a bandgap, field-effect transistors based on this material can be turned off⁴. These transistors demonstrate a current ON/OFF ratio of $\sim 1 \times 10^8$, low subthreshold swing (74 mV dec -'1) and negligible OFF current (25 fA µm⁻¹)⁴. Logic circuits¹⁹ and amplifiers²⁰ based on monolayer MoS₂ have also been demonstrated recently, as well as saturation and high breakdown currents²¹.

The direct bandgap^{7,8} of monolayer MoS₂ suggests that it could be a promising material for optoelectronic applications. Its most

basic application would be as a semiconducting channel in phototransistors, where light would be directly converted into current. However, the photoresponsivity of previously demonstrated mono- and multilayer transistors is relatively low, with the first monolayer $\rm MoS_2$ phototransistors exhibiting a photoresponsivity of 7.5 mA W $^{-1}$ (ref. 22), which is comparable to graphene-based devices with a similar geometry (6.1 mA W $^{-1}$) 23 . Recently reported multilayer $\rm MoS_2$ devices 24,25 show higher photoresponsivities, on the order of $\sim\!100$ mA W $^{-1}$, which is comparable to silicon-based photodetectors. The relatively low mobility (0.1 cm 2 V $^{-1}$ s $^{-1}$) and device currents (1–100 nA) in these first monolayer devices could offset the inherent advantage of using a material with a direct bandgap.

Here, we demonstrate an ultrasensitive monolayer MoS_2 photodetector with a photoresponsivity reaching 880 A W^{-1} , which is a 100,000-fold improvement over previous reports for monolayer MoS_2 phototransistors²². This is a consequence of its improved mobility, as well as the contact quality and positioning technique. Because of the direct bandgap, our ultrasensitive MoS_2 photodetectors have a photoresponsivity that is $\sim 10^6$ better than the first graphene photodetectors ($\sim 0.5 \text{ mA W}^{-1}$)²⁶. The direct nature of the bandgap in monolayer MoS_2 in contrast to the indirect bandgap in bulk MoS_2 also results in an $\sim 9,000$ -fold higher photoresponsivity in monolayer MoS_2 compared to that in multilayer devices²⁵.

We began the fabrication of our devices by using the scotch-tape based micromechanical cleavage method to exfoliate monolayer MoS₂ (refs 3,27). As a substrate, we used degenerately doped silicon onto which a 270-nm-thick layer of SiO₂ had been grown (Fig. 1a). We tested various surface treatments and their effects on the photoresponse and the rise and fall times (see Supplementary Fig. S2 for more information and a comparison between different substrate treatments). Unless otherwise noted, we used a 30 min soak in 30 vol% KOH to remove a <5 nm thin surface layer of SiO₂, followed by oxygen plasma cleaning to further clean and activate the surface. After exfoliation, we located monolayer MoS₂ flakes based on their optical contrast with respect to the underlying SiO₂ layer²⁸. We have previously established the correlation between contrast and thickness as measured by atomic force microscopy²⁸. Electron-beam lithography and metal evaporation were used for the fabrication of 90-nm-thick gold electrodes (Fig. 1b). This was followed by a 2 h annealing step at 200 °C in an argon atmosphere²⁹, after which the devices were wire-bonded and loaded in the measurement setup.

We probed the devices and their time-dependent photoresponse to laser excitation using a focused laser beam ($\lambda = 561$ nm) and an illumination power of 15 μ W (Fig. 1c). A microscope objective and a micromechanical stage were used to localize the device, and a nanopositioning stage was used for photocurrent map generation. The spot size had a diameter of 2.8 μ m, resulting in an estimated maximum illumination intensity of ~238 W cm⁻². Before any

¹Electrical Engineering Institute, Ecole Polytechnique Federale de Lausanne (EPFL), CH-1015 Lausanne, Switzerland, ²Institute of Biotechnology, Ecole Polytechnique Federale de Lausanne (EPFL), CH-1015 Lausanne, Switzerland. *e-mail: aleksandra.radenovic@epfl.ch; andras.kis@epfl.ch

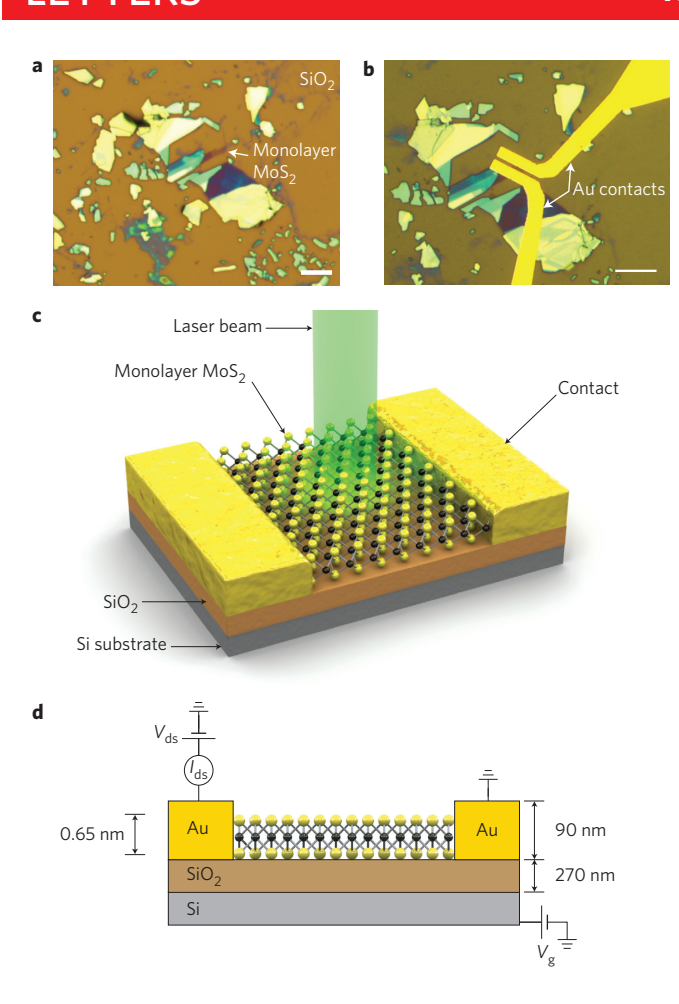


Figure 1 | Monolayer MoS₂ phototransistor layout. **a**, Optical image of the single-layer MoS₂ flake serving as the conductive channel in our photodetector. Scale bar, 10 μm. **b**, Optical image of the device based on the flake shown on **a**. Scale bar, 10 μm. The device consists of a field-effect transistor with two gold contacts and gated using a degenerately doped silicon substrate. **c**, Three-dimensional schematic view of the single-layer MoS₂ photodetector and the focused laser beam used to probe the device. **d**, Cross-sectional view of the structure of the single-layer MoS₂ photodetector together with electrical connections used to characterize the device. A single layer of MoS₂ (6.5 Å thick) is deposited on a degenerately doped silicon substrate with a 270-nm-thick SiO₂ layer. The substrate acts as a backgate. One of the gold electrodes acts as drain while the other, the source electrode, is grounded.

device characterization we generated a photocurrent map to establish optimal x, y and z locations for the focused laser beam spot. In addition to an optimized surface treatment and improved contacts, localization of the highest photocurrent response on the device results in the ultrasensitive response of our device.

The device was electrically characterized by applying a constant drain–source voltage $V_{\rm ds}$ and a backgate voltage $V_{\rm g}$ in the configuration shown in Fig. 1d. From the backgate voltage sweep, we estimate an effective field-effect mobility μ of \sim 4 cm 2 V $^{-1}$ s $^{-1}$, typical for monolayer MoS $_2$ devices 3,4 .

We now explore the spatial extent of the photosensitive region in our device. Figure 2a shows the spatially resolved photocurrent map acquired by scanning the focused laser beam ($\lambda = 561$ nm) across the sample. The beam was modulated at 571 Hz using a mechanical chopper. The map clearly shows that photocurrent generation occurs in the area centred on the MoS $_2$ flake. All subsequent measurements were performed by locating the laser beam in the region with the highest photoresponse.

Electrical characterization was repeated under different illumination intensities in the 150 pW to 15 $\mu\rm W$ range with a green laser ($\lambda=561$ nm; Fig. 2b). The $I_{\rm ds}-V_{\rm ds}$ curves shown in Fig. 2b are linear and symmetric for small bias voltages, indicating an ohmic-like contact, and show an increase of drain current by several orders of magnitude as the device is illuminated. As a consequence, the photocurrent $I_{\rm ph}$ ($I_{\rm ph}=I_{\rm illuminated}-I_{\rm dark}$) also increases with bias voltage $V_{\rm ds}$ due to the increase in carrier drift velocity and related reduction of the carrier transit time $T_{\rm t}$ (defined as $T_{\rm t}=l^2/\mu V_{\rm ds}$, where l is the device length, μ is the carrier mobility and $V_{\rm ds}$ is the bias voltage).

We recorded the dependence of photocurrent generation on backgate voltage, reported in Fig. 2c for an incident illumination power ($P_{\rm inc}$) of 0.15 μ W. In the dark state, our device shows behaviour typical of MoS₂-based field-effect transistors with an n-type channel and a threshold voltage of $V_{\rm t}=22$ V. When we illuminated the device biased at $V_{\rm ds}=8$ V using a focused laser beam, the OFF current increased into the \sim 4 μ A range, with the device current increasing for both the ON and OFF states for all values of gate voltage. This indicates that the photocurrent dominates over thermionic and tunnelling currents in the entire operating range of the device.

We then explored the spectral response of our device, expressed through its external photoresponsivity R, defined as the ratio of the photocurrent and the incident illumination power (that is, $I_{\rm ph}/P_{\rm inc}$). The dependence of the photoresponsivity on illumination wavelength for a similar monolayer ${\rm MoS_2}$ device is plotted in Fig. 2d. The photoresponsivity is negligible for wavelengths above ${\sim}680$ nm, corresponding to a photon energy ${\sim}1.8$ eV, which corresponds to the bandgap of monolayer ${\rm MoS_2}$ (ref. 8). Decreasing the excitation wavelength to ${<}680$ nm results in the excitation of electrons from the valence to the conduction band and the generation of photocurrent. The transition probability increases for higher photon energies, which is reflected in the monotonous increase of the photocurrent down to a 400 nm excitation wavelength.

The observed behaviour of our photodetector can be explained by a simple energy band diagram (Fig. 2e). With no illumination and without applying gate or drain bias, the device is in its equilibrium state, characterized by small Schottky barriers at the contacts 30 . Illuminating the device in its OFF state ($V_{\rm g} < V_{\rm t}$), with light characterized by wavelengths <680 nm, results in light absorption and excitation of electron–hole pairs, which can be extracted by applying a drain–source bias. The photocurrent increases linearly with applied bias $V_{\rm ds}$ due to the reduction of the carrier transit time. In the ON state ($V_{\rm g} > V_{\rm t}$), in addition to the photogenerated current, thermionic and tunnelling currents also contribute to the device currents. Increasing the gate voltage lowers the barriers at the contacts, resulting in a more efficient photocurrent extraction and increased photoresponse. Operating the device in the OFF state brings the advantage of a reduced dark current.

One of the most important figures of merit for a photodetector is its external photoresponsivity R. Figure 3 shows the photocurrent $I_{\rm ph}$ and photoresponsivity R acquired at a bias voltage of $V_{\rm ds}=8$ V and a backgate voltage of $V_{\rm g}=-70$ V. At low illumination intensities (150 pW), the device reaches a photoresponsivity of 880 A W $^{-1}$, $\sim 10^6$ times higher than the first graphene photodetectors 26 and 100,000 times higher than previous reports for monolayer MoS $_2$ phototransistors 22 . To determine the sensitivity of our photodetector, we measured the noise in the dark current, giving a noise-equivalent power (NEP) of 1.8×10^{-15} W Hz $^{-1/2}$ for $V_{\rm ds}=8$ V and a backgate voltage of $V_{\rm g}=-70$ V (see Supplementary Fig. S3 for more details). For comparison, commercial state-of-the-art silicon avalanche photodiodes based on p-n junctions have an NEP of 3×10^{-14} W Hz $^{-1/2}$ (ref. 31), limited by the shot noise of the dark current. Photodiodes based on p-n junctions are in general more sensitive than phototransistors based on just one

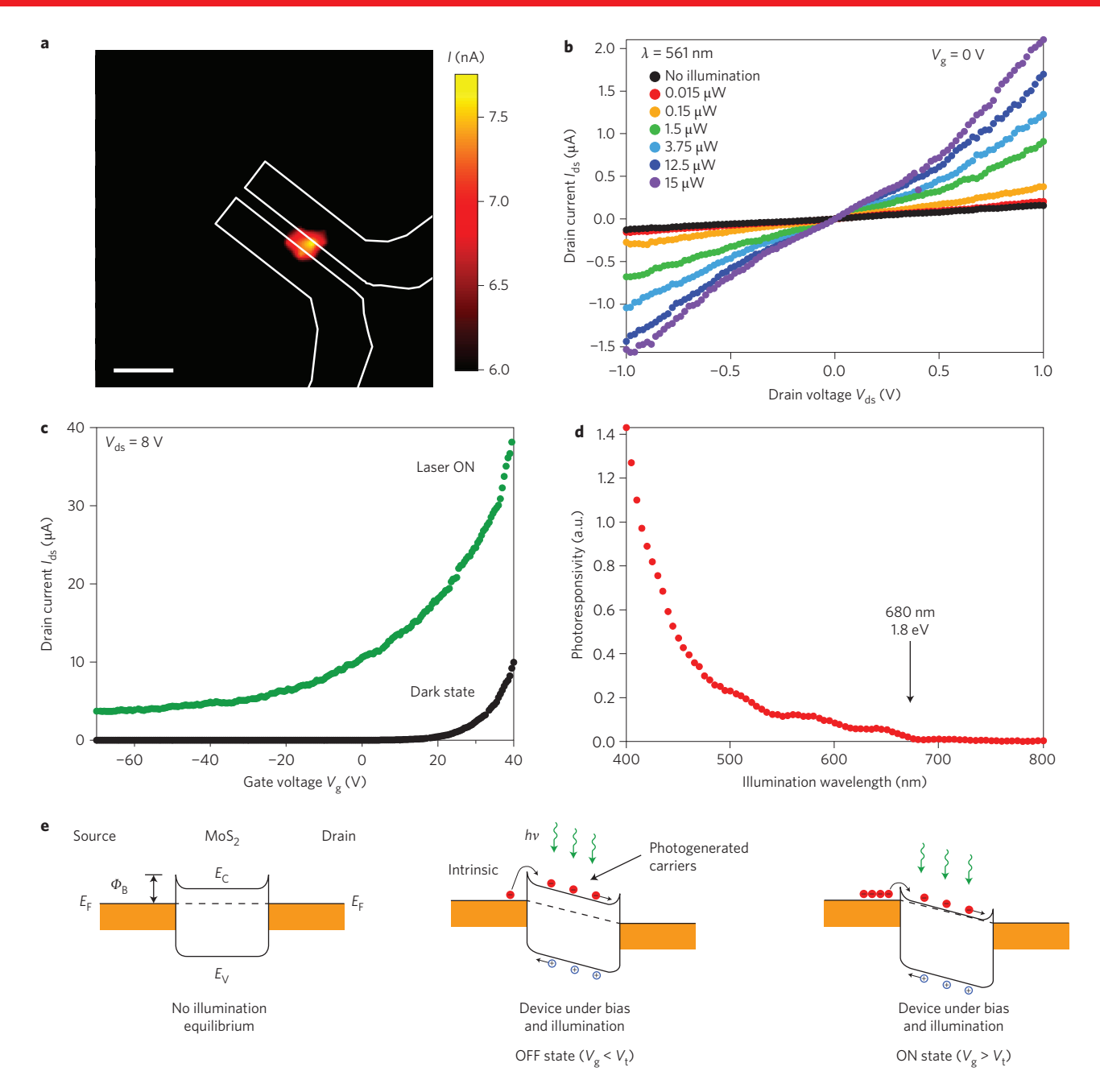


Figure 2 | Photoinduced response of the single-layer MoS₂ photodetector. a, Spatial map of the photocurrent recorded as a focused laser beam is raster-scanned over the surface of the photodetector using a nanopositioning stage. Scale bar, 5 μm. $V_{ds} = 1$ V, $V_g = 0$ V, $P_{inc} = 0.425$ μW. The spatial profile shows that light detection is confined to a small area centred on the MoS₂ flake. **b,** Drain-source (I_{ds} - V_{ds}) characteristic of the device in the dark and under different illumination intensities. The device operates as an enhancement-mode transistor. Increasing illumination levels result in enhanced current due to electron-hole pair generation by light absorption in the direct bandgap of monolayer MoS₂. **c,** Gating response (I_{ds} - V_g) of the MoS₂ photodetector in dark and illuminated states, acquired for a backgate voltage V_g between -70 V and +40 V. Illumination power is 0.15 μW. **d,** Photoresponsivity of a similar monolayer MoS₂ device as a function of illumination wavelength. The device shows a uniformly increasing response as the illumination wavelength is reduced from 680 nm to 400 nm and indicates that monolayer MoS₂ photodetectors can be used for a broad range of wavelengths. **e,** Band diagram of the monolayer MoS₂ photodetector taking into consideration small Schottky barriers at the contacts. E_F is the Fermi level energy, E_C the minimum conduction band energy, E_C the maximum valence band energy and Φ_B the Schottky barrier height. There is no electrical current flowing under equilibrium conditions and no illumination. Photocurrent is generated under illumination and is the dominant channel current in the OFF state, with thermionic and tunnelling currents being negligible. Thermionic and tunnelling currents contribute in the ON-state of the device.

type of semiconductor. In contrast to silicon photodiodes, our device consists of a simple n-type channel, which is easier to manufacture than a p-n junction and could therefore lead to reduced production costs. The high sensitivity arises from the low OFF-state current due to the 1.8 eV bandgap and also the high degree of electrostatic control over the atomically thick channel, as well

as highly efficient carrier excitation, also due to the direct bandgap. In the case of our device, the equivalent dark current shot noise, $\sqrt{2eI_{\rm dark}}$, is $8\times 10^{-16}\,{\rm A~Hz^{-1/2}}$ for $I_{\rm dark}=2~{\rm pA}$ (the OFF-state current in our device), indicating that there is room for further improvement and that single-layer MoS $_2$ could have great potential for high-sensitivity applications.

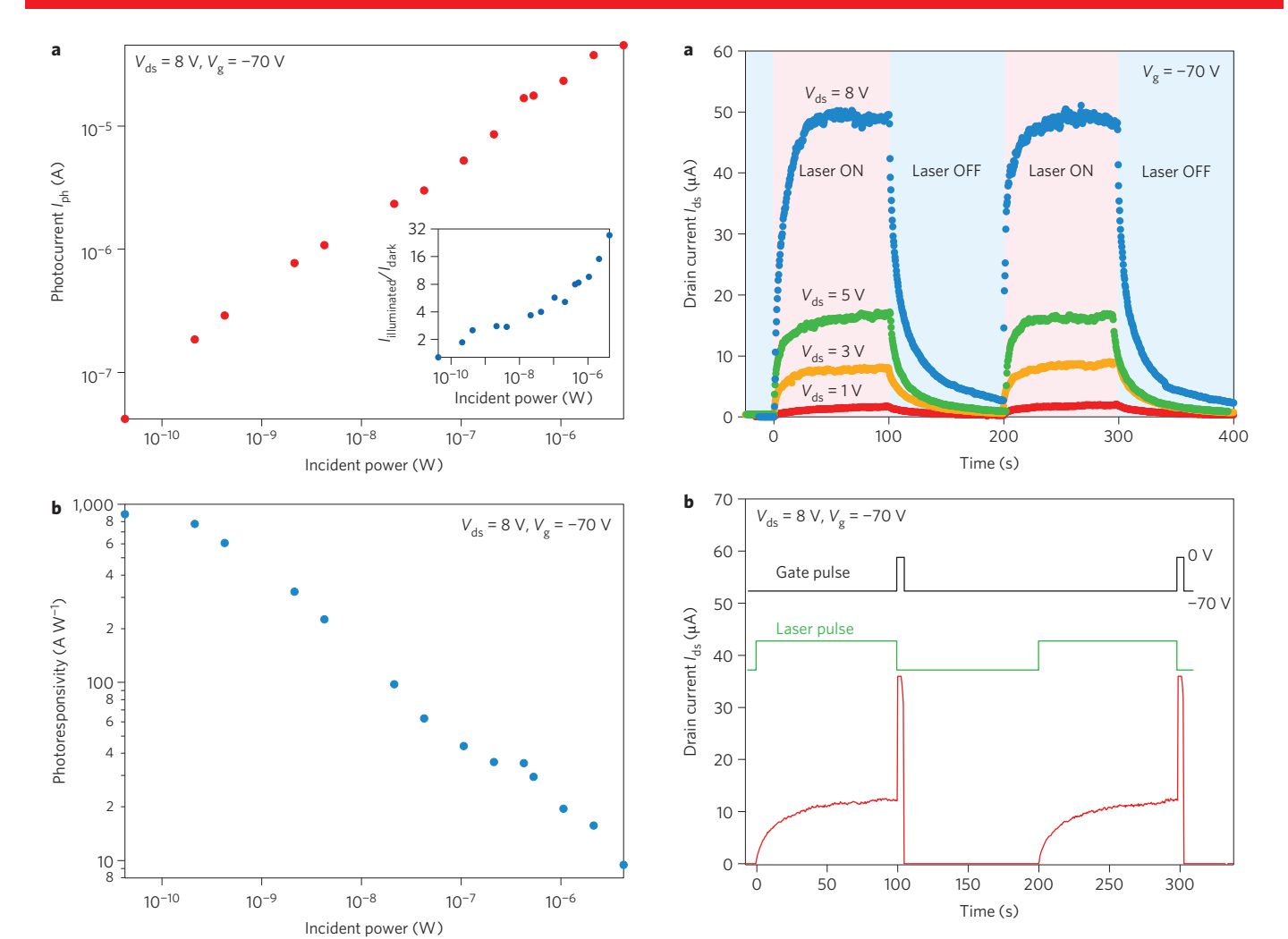


Figure 3 | Dependence of photoresponse on illumination intensity. a, Photocurrent of the monolayer MoS_2 phototransistor for bias voltage $V_{ds}=8\ \text{V}$ and gate voltage $V_g=-70\ \text{V}$, corresponding to the OFF state of the transistor. Inset: ratio of device currents in illuminated and dark states for different illumination powers. **b**, Photoresponsivity of the MoS_2 phototransistor, showing high sensitivity. The device exhibits a photoresponsivity of 880 A W $^{-1}$ for an illumination power of 150 pW ($\sim\!24\ \mu\text{W}\ \text{cm}^{-2}$) and shows a monotonous decrease with increasing illumination intensity due to the saturation of trap states present either in MoS_2 or at the $\text{MoS}_2/\text{substrate}$ interface.

As the light intensity is increased, the photocurrent demonstrates a sublinear dependence on it. This reduction in photoresponsivity can be explained in terms of trap states present either in MoS₂ or at the interface between the MoS₂ and the underlying SiO₂ layer³². This is exacerbated by the high surface-to-volume ratio of the MoS₂. Under high illumination intensities the density of available states is reduced, resulting in saturation of the photoresponse. The presence of trap states can dramatically influence the dynamics of the MoS₂ photodetector, which can be studied using time-resolved measurements. In Fig. 4a we plot, for four different bias voltages, the rise in photocurrent upon turning on the laser light ($\lambda = 561 \text{ nm}$) and its decay after removing the incident light. The response is characterized by a typical rise time of $\tau_{\text{rise}} = 4 \text{ s}$ and $\tau_{\text{decay}} = 9 \text{ s}$ for $V_{\rm ds} = 8 \text{ V}$ and $V_{\rm g} = -70 \text{ V}$, where the rising and falling parts of the curve can be fitted using a single exponential function. The slow components of the photocurrent rise (τ_{rise}) and decay (τ_{decay}) times reported in this study are similar to the corresponding values hybrid graphene-quantum observed in

Figure 4 | Photocurrent dynamics. a, Time-resolved photoresponse of the device, recorded for different values of bias voltage $V_{\rm ds}$ and $P_{\rm inc}=4.25~\mu{\rm W}$. The laser light is first turned on for a period of 100 s, then turned off for 100 s. Both the rise and fall in photocurrent can be fitted using single exponential functions, resulting in $\tau_{\rm rise}=4~{\rm s}$ and $\tau_{\rm decay}=9~{\rm s}$ for $V_{\rm ds}=8~{\rm V}$. **b**, Time-resolved photoresponse of the device (red curve) to an incident power of 0.425 $\mu{\rm W}$, with application of a reset voltage pulse to the gate electrode. The fall time is reduced to less than 0.6 s.

phototransistors³³. They are also orders of magnitude shorter than values reported for phototransistors based on amorphous oxide semiconductors³⁴. The surroundings of the MoS₂ play an important role in photocurrent dynamics, with various surface treatments able to modify the decay time in the 0.3–4,000 s range, possibly due to differences in surface hydrophobicity^{35,36} (Supplementary Fig. S2). We can also improve the response time by applying a short gate pulse (Fig. 4b) consisting of a brief increase in gate voltage from –70 V to 0 V. This causes a discharge of trapped charge carriers^{33,34} and results in a decrease in the photocurrent decay time for this device to less than 0.6 s, which is the temporal resolution of our measurement. Further studies and device optimization will be performed to improve the photocurrent dynamics of monolayer MoS₂ devices. Important enhancements could be realized using encapsulation and surface trap state passivation.

To summarize, we have fabricated phototransistors based on monolayer MoS₂. Because of the direct bandgap of monolayer MoS₂, devices based on it exhibit a very high photoresponsivity, reaching 880 A W⁻¹ and surpassing previous reports for monolayer MoS₂ by a factor of 100,000 and for first graphene photodetectors by

a factor of $\sim 10^6$. The photodetector has a broad spectral range, with photocurrent monotonously increasing as the wavelength of the incident light is decreased from 680 nm to 400 nm. Furthermore, the presence of a bandgap and the high degree of electrostatic control due to the atomic-scale thickness allows the phototransistor to be turned off, resulting in low dark currents and NEP lower than in commercial state-of-the-art silicon avalanche photodiodes³¹. This makes monolayer MoS₂ a promising semiconducting material for applications in optoelectronics. Rather than an intrinsic limitation slow photoresponse dynamics is the most important limiting factor, but this could be overcome by MoS₂/substrate engineering to reduce charge trap density and is a technical challenge rather than an intrinsic limitation. Another important technological step would be to integrate MoS2 phototransistors with conventional complementary metal-oxide-semiconductor (CMOS) imaging circuitry. Possible fields of applications could include consumer imaging sensors suitable for low-light photography, for example in cell-phone cameras, which currently suffer from poor low-light performance, or in sensors for fluorescence imaging. Combining our results with large-area material preparation methods such as liquid scale exfoliation^{11,12} or CVD growth^{14,15}, together with the simplicity of the device presented here, could also result in the fabrication of inexpensive, high-sensitivity and flexible MoS₂ optoelectronic devices.

Materials and methods

All measurements were performed under ambient conditions. Single layers of ${\rm MoS}_2$ were exfoliated from commercially available crystals of molybdenite (SPI Supplies Brand Moly Disulfide) using the scotch-tape micromechanical cleavage technique pioneered for the production of graphene¹. Electrical measurements (d.c.) were carried out using a National Instruments DAQ card and Stanford Research SR560 current preamplifier. Photocurrent maps were acquired by modulating the laser beam with a mechanical chopper (571 Hz) and detecting the photocurrent with a current preamplifier and a lock-in amplifier. A monochromator was used for wavelength-dependent measurements of the photocurrent.

Received 24 September 2012; accepted 26 April 2013; published online 9 June 2013

References

- Novoselov, K. S. et al. Electric field effect in atomically thin carbon films. Science 306, 666–669 (2004).
- Dean, C. R. et al. Boron nitride substrates for high-quality graphene electronics. Nature Nanotech. 5, 722–726 (2010).
- 3. Novoselov, K. S. et al. Two-dimensional atomic crystals. Proc. Natl Acad. Sci. USA 102, 10451–10453 (2005).
- Radisavljevic, B., Radenovic, A., Brivio, J., Giacometti, V. & Kis, A. Single-layer MoS₂ transistors. *Nature Nanotech.* 6, 147–150 (2011).
- Fang, H. et al. High-performance single layered WSe₂ p-FETs with chemically doped contacts. Nano Lett. 12, 3788–3792 (2012).
- Liu, W. et al. Role of metal contacts in designing high-performance monolayer n-type WSe₂ field effect transistors. Nano Lett. 13, 1983–1990 (2013).
- Splendiani, A. et al. Emerging photoluminescence in monolayer MoS₂. Nano Lett. 10, 1271–1275 (2010).
- Mak, K. F., Lee, C., Hone, J., Shan, J. & Heinz, T. F. Atomically thin MoS₂: a new direct-gap semiconductor. *Phys. Rev. Lett.* 105, 136805 (2010).
- Lebegue, S. & Eriksson, O. Electronic structure of two-dimensional crystals from ab initio theory. Phys. Rev. B 79, 115409 (2009).
- Kuc, A., Zibouche, N. & Heine, T. Influence of quantum confinement on the electronic structure of the transition metal sulfide TS₂. *Phys. Rev. B* 83, 245213 (2011).
- Coleman, J. N. et al. Two-dimensional nanosheets produced by liquid exfoliation of layered materials. Science 331, 568–571 (2011).
- Smith, R. J. et al. Large-scale exfoliation of inorganic layered compounds in aqueous surfactant solutions. Adv. Mater. 23, 3944–3948 (2011).
- 13. Lee, K. et al. Electrical characteristics of molybdenum disulfide flakes produced by liquid exfoliation. Adv. Mater. 23, 4178–4182 (2011).
- 14. Liu, K-K. et al. Growth of large-area and highly crystalline MoS_2 thin layers on insulating substrates. Nano Lett. 12, 1538–1544 (2012).

- Zhan, Y., Liu, Z., Najmaei, S., Ajayan, P. M. & Lou, J. Large-area vaporphase growth and characterization of MoS₂ atomic layers on a SiO₂ substrate. Small 8, 966–971 (2012).
- Brivio, J., Alexander, D. T. L. & Kis, A. Ripples and layers in ultrathin MoS₂ membranes. Nano Lett. 11, 5148–5153 (2011).
- Bertolazzi, S., Brivio, J. & Kis, A. Stretching and breaking of ultrathin MoS₂. ACS Nano 5, 9703–9709 (2011).
- Kam, K. K. & Parkinson, B. A. Detailed photocurrent spectroscopy of the semiconducting group VIB transition metal dichalcogenides. *J. Phys. Chem.* 86, 463–467 (1982).
- Radisavljevic, B., Whitwick, M. B. & Kis, A. Integrated circuits and logic operations based on single-layer MoS₂. ACS Nano 5, 9934–9938 (2011).
- Radisavljevic, B., Whitwick, M. B. & Kis, A. Small-signal amplifier based on single-layer MoS₂. Appl. Phys. Lett. 101, 043103 (2012).
- Lembke, D. & Kis, A. Breakdown of high-performance monolayer MoS₂ transistors. ACS Nano 6, 10070–10075 (2012).
- Yin, Z. et al. Single-layer MoS₂ phototransistors. ACS Nano 6, 74–80 (2011).
 Mueller, T., Xia, F. & Avouris, P. Graphene photodetectors for high-speed optical communications. Nature Photon. 4, 297–301 (2010).
- Lee, H. S. et al. MoS₂ nanosheet phototransistors with thickness-modulated optical energy gap. Nano Lett. 12, 3695–3700 (2012).
- Choi, W. et al. High-detectivity multilayer MoS₂ phototransistors with spectral response from ultraviolet to infrared. Adv. Mater. 24, 5832–5836 (2012).
- Xia, F., Mueller, T., Lin, Y-m., Valdes-Garcia, A. & Avouris, P. Ultrafast graphene photodetector. *Nature Nanotech.* 4, 839–843 (2009).
- Frindt, R. F. Single crystals of MoS₂ several molecular layers thick. J. Appl. Phys. 37, 1928–1929 (1966).
- Benameur, M. M. et al. Visibility of dichalcogenide nanolayers. Nanotechnology 22, 125706 (2011).
- Ishigami, M., Chen, J. H., Cullen, W. G., Fuhrer, M. S. & Williams, E. D. Atomic structure of graphene on SiO₂. Nano Lett. 7, 1643–1648 (2007).
- Liu, H., Neal, A. T. & Ye, P. D. Channel length scaling of MoS₂ MOSFETs. ACS Nano 6, 8563–8569 (2012).
- Krainak, M. A., Sun, X., Yang, G. & Lu, W. Comparison of linear-mode avalanche photodiode lidar receivers for use at one-micron wavelength. *Proc. SPIE* 7681, 76810Y (2010).
- Ghatak, S., Pal, A. N. & Ghosh, A. Nature of electronic states in atomically thin MoS₂ field-effect transistors. ACS Nano 5, 7707–7712 (2011).
- 33. Konstantatos, G. et al. Hybrid graphene-quantum dot phototransistors with ultrahigh gain. *Nature Nanotech.* 7, 363–368 (2012).
- Jeon, S. et al. Gated three-terminal device architecture to eliminate persistent photoconductivity in oxide semiconductor photosensor arrays. Nature Mater. 11, 301–305 (2012).
- 35. Nagashio, K., Yamashita, T., Nishimura, T., Kita, K. & Toriumi, A. Electrical transport properties of graphene on ${\rm SiO_2}$ with specific surface structures. *J. Appl. Phys.* **110**, 024513 (2011).
- Late, D. J., Liu, B., Matte, R. H. S. S., Dravid, V. P. & Rao, C. N. R. Hysteresis in single-layer MoS₂ field effect transistors. ACS Nano 6, 5635–5641 (2012).

Acknowledgements

The authors thank B. Radisavljevic for advice regarding device fabrication and A. Fontcuberta i Morral for the use of the monochromator. Device fabrication was carried out partly in the EPFL Center for Micro/Nanotechnology (CMI). Thanks go to Z. Benes (CMI) for technical support with electron-beam lithography. This work was financially supported by the Swiss Nanoscience Institute (NCCR Nanoscience) and the European Research Council (grant no. 240076; FLATRONICS: Electronic devices based on nanolayers; grant no. 259398; PorABEL: Nanopore integrated nanoelectrodes for biomolecular manipulation and sensing).

Author contributions

O.L.S. and D.L. worked on device fabrication. O.L.S. performed the measurements and analysed the data. A.R. and M.K. built the optical setup. O.L.S., D.L., A.R. and A.K. designed the experiment. O.L.S., A.K. and A.R. wrote the manuscript.

Additional information

Supplementary information is available in the online version of the paper. Reprints and permissions information is available online at www.nature.com/reprints. Correspondence and requests for materials should be addressed to A.R. or A.K.

Competing financial interests

The authors declare no competing financial interests.

SUPPLEMENTARY INFORMATION

DOI: 10.1038/NNANO.2013.100

1

Supplementary information for Ultrasensitive photodetectors based on monolayer MoS₂

Oriol Lopez-Sanchez¹, Dominik Lembke¹, Metin Kayci², Aleksandra Radenovic², Andras Kis^{1*}

¹Electrical Engineering Institute, Ecole Polytechnique Federale de Lausanne (EPFL), CH-1015 Lausanne, Switzerland

²Institute of Biotechnology, Ecole Polytechnique Federale de Lausanne (EPFL), CH-1015 Lausanne, Switzerland

*Correspondence should be addressed to: AndrasKis, andras.kis@epfl.ch

DEVICE MOBILITY MEASUREMENTS

The device is first characterized in the dark state by applying a constant drain-source voltage $V_{\rm ds} = 100$ mV and sweeping the back-gate voltage $V_{\rm bg}$. The effective field-effect mobility of the device with 90 nm Au contacts and KOH/O₂plasma surface pretreatment is estimated from the back gate sweep using the equation $\Box = [dI_{DS}/dV_{BG}] \times [L/WC_iV_{DS}]$ where L=1 μ m is the channel length, W = 2 μ m channel width C_i = 1.3×10⁻⁴Fm⁻² the back gate capacitance (C_i = $\epsilon_0\epsilon_r/d$; ϵ_r = 3.9, d = 270 nm). For the device shown in Figure 1a in the manuscript, we obtain the field-effect mobility μ = 4 cm²/Vs, typical of monolayer MoS₂ devices. 1,2

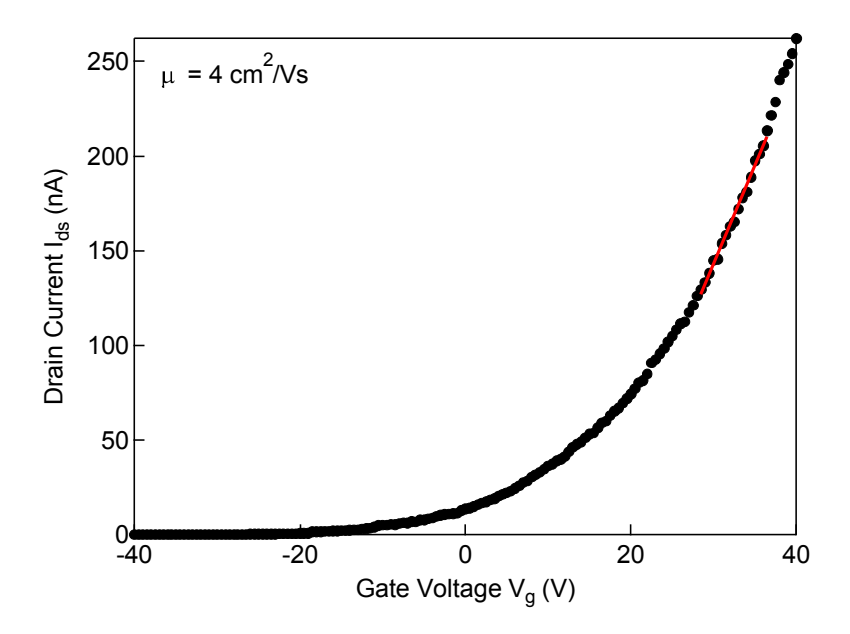


Figure S1. Gating characteristics of the monolayer MoS_2 transistor presented in the main manuscript. Room-temperature transfer characteristic of the monolayer MoS_2 phototransistor presented in the main manuscript. I_{ds} - V_g sweep is performed at V_{ds} =100 mV.

SUBSTRATE INFLUENCE ON THE DECAY TIME AND RESPONSIVITY

We studied the influence of different pre-deposition surface treatments and contact materials on the photoresponse decay. We find that different surface cleaning treatments can be used to reduce the decay time. This can be explained by differences in resulting level of hydrophobicity of the functionalized SiO_2 surface.³ Using a different growth technique to deposit SiO_2 (wet vs. dry oxidation) results in further decrease of the characteristic decay time τ_{decay} . We used the following SiO_2 surface treatments preceding micromechanical exfoliation:

 $KOH - SiO_2$ substrates were soaked for 30 min in a 30% KOH solution in water at room temperature. This was followed by 20 min O_2 plasma treatment with an RF power of 270 W, followed by exfoliation.

Piranha - SiO₂ substrates were soaked for 45 min in a piranha cleaning solution (H₂SO₄:H₂O₂ 3:1). This was followed by 20 min O2 plasma treatment with an RF power of 270 W, followed by exfoliation.

HF - SiO₂ substrates were soaked for 30 sec in 2 ml 50% vol of HF with 70 ml of DI-water. This was followed by 20 min O2 plasma treatment with an RF power of 270 W, followed by exfoliation.

Using different contacting metals such as Ti/Au (10/50nm) or Cr/Au (10/50nm)results on further decrease of the decay time but at the expense of photoresponsivity with the lowest decay time τ_{decay} reaching 320 ms for a device employing Cr/Au contacts and SiO₂ grown using wet oxidation.

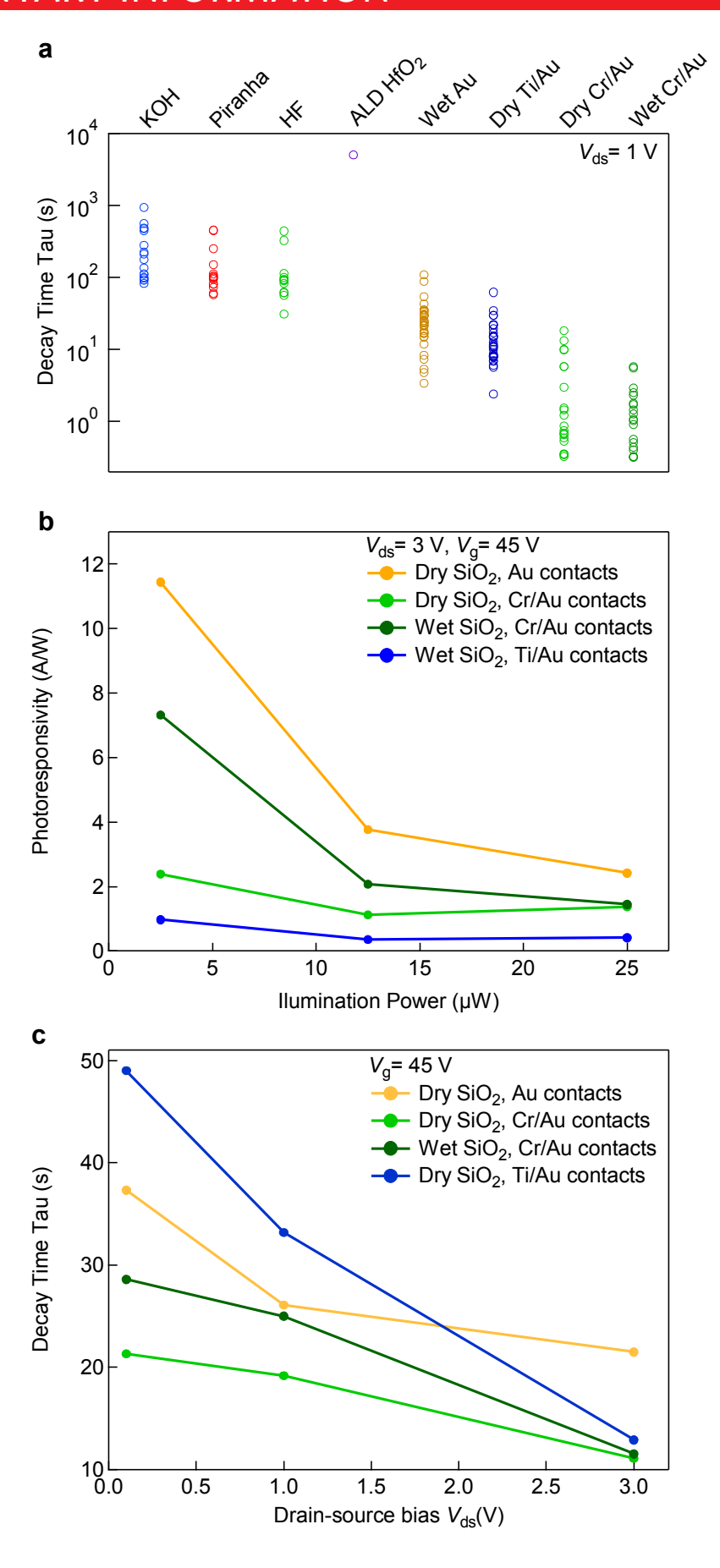


Figure S2. Photoresponse dynamics. a, Photoresponse decay times recorded for devices exposed to a broad white light of Olympus KL 1500 LCD of 0.073 W/cm² with various surface treatments and contact materials, including a deposition of 30 nm HfO₂ layer on top of MoS₂, grown by atomic layer deposition (ALD). **b,** Dependence of the photoresponse decay time on the drain-source bias V_{ds} recorded for samples exposed to 561 nm laser with 2 μm spot size with different surface treatments and contact materials. We find no significant dependence of the photoresponse on the gate voltage V_g . **c,** Dependence of the photoresponsivity on the illumination power recorded for samples with different surface treatments and contact materials exposed to 561 nm laser with a 2 μm spot size.

DETERMINATION OF THE NOISE EQUIVALENT POWER (NEP)

In order to calculate the noise equivalent power (NEP) of the single-layer MoS₂ phototransistor, we measure the dark current of the device with a source-drain voltage $V_{\rm ds} = 8$ V and back-gate voltage $V_{\rm g} = -70$ V. The noise power spectrum is shown on Figure S3. At 1Hz, we get $S(f = 1\text{Hz}) = 2.42 \times 10^{-24} \text{ A}^2 \text{ Hz}^{-1}$. With the responsivity R = 880 A/W we extract a NEP of $1.8 \times 10^{-15} \text{ W Hz}^{-1/2}$.

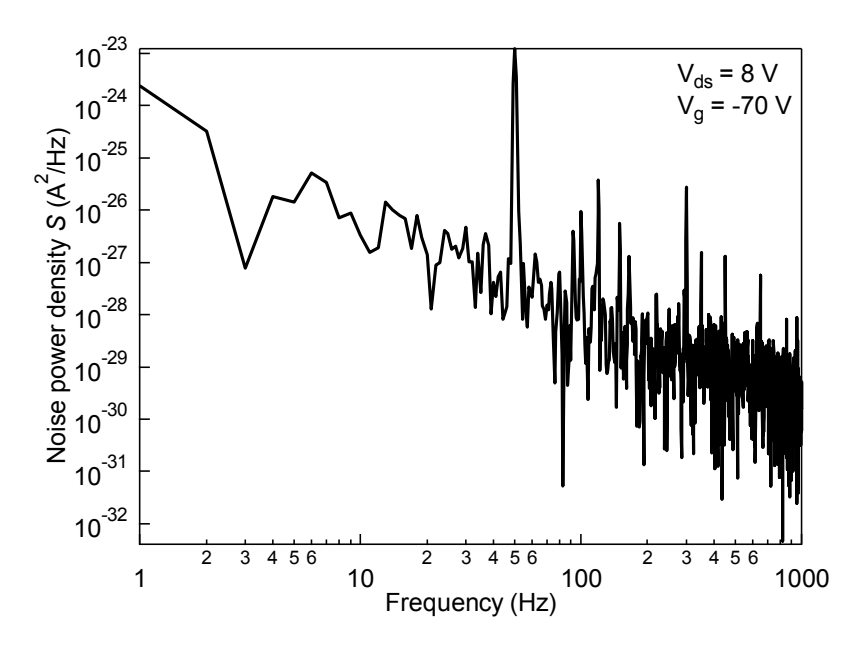


Figure S3. Noise level determination. Noise power density of the dark current of the single-layer MoS_2 photodetector measured for V_{ds} = 8 V and back-gate voltage V_g = -70 V, corresponding to the same conditions in which we measured its photoresponsitivty.

REFERENCES

- 1 Novoselov, K. S. *et al.* Two-dimensional atomic crystals. *PNAS* **102**, 10451-10453, (2005).
- 2 Radisavljevic, B., Radenovic, A., Brivio, J., Giacometti, V. & Kis, A. Single-layer MoS₂ transistors. *Nature Nanotech.* **6**, 147-150, (2011).
- Nagashio, K., Yamashita, T., Nishimura, T., Kita, K. & Toriumi, A. Electrical transport properties of graphene on SiO₂ with specific surface structures. *J. App. Phys.* **110**, 024513, (2011).